Journal of Power Sources 241 (2013) 423–428

Contents lists available at SciVerse ScienceDirect

Journal of Power Sources

journal homepage: www.elsevier.com/locate/jpowsour

Polyaniline modified graphene and carbon nanotube composite electrode for asymmetric supercapacitors of high energy density

Qian Cheng [a,b], Jie Tang [a,b,**], Norio Shinya [b], Lu-Chang Qin [c,*]

[a] National Institute for Materials Science, 1-2-1 Sengen, Tsukuba 305-0047, Japan
[b] Doctoral Program in Materials Science and Engineering, University of Tsukuba, 1-1-1 Tennodai, Tsukuba 305-8577, Japan
[c] Department of Physics and Astronomy, University of North Carolina at Chapel Hill, Chapel Hill, NC 27599-3255, USA

HIGHLIGHTS

- Fabrication and characterization of graphene composite structure as supercapacitor electrodes.
- Energy density of 188 Wh kg^{-1} has been obtained.
- Graphene composite with carbon nanotubes and PANI components leads to high device performance.

ARTICLE INFO

Article history:
Received 1 February 2013
Received in revised form
20 April 2013
Accepted 22 April 2013
Available online 30 April 2013

Keywords:
Supercapacitor
Graphene
Carbon nanotube
PANI

ABSTRACT

Graphene and single-walled carbon nanotube (CNT) composites are explored as the electrodes for supercapacitors by coating polyaniline (PANI) nano-cones onto the graphene/CNT composite to obtain graphene/CNT–PANI composite electrode. The graphene/CNT–PANI electrode is assembled with a graphene/CNT electrode into an asymmetric pseudocapacitor and a highest energy density of 188 Wh kg^{-1} and maximum power density of 200 kW kg^{-1} are achieved. The structure and morphology of the graphene/CNT composite and the PANI nano-cone coatings are characterized by both scanning electron microscopy and transmission electron microscopy. The excellent performance of the assembled supercapacitors is also discussed and it is attributed to (i) effective utilization of the large surface area of the three-dimensional network structure of graphene-based composite, (ii) the presence of CNT in the composite preventing graphene from re-stacking, and (ii) uniform and vertically aligned PANI coating on graphene offering increased electrical conductivity.

1. Introduction

With the rapid growth of portable electronics, electric vehicles (EV), and hybrid electric vehicles (HEV), there have been increasing demands of high-performance energy storage devices. Supercapacitors, which are also known as electrochemical capacitors or electric double-layer capacitors, offer a promising alternative to meet the increasing power demand of energy storage systems [1,2]. Supercapacitors have attracted much renewed attention in recent years because of their pulse high power supply, long cycle life (>100,000 cycles), simple operational mechanism, and high dynamics of charge propagation, and these characteristics have made supercapacitors an ideal energy storage device for applications requiring short load cycle and high reliability [3]. Depending on the electrode material and the operational mechanism of supercapacitors, there are three major types of supercapacitors that have attracted intensive activities in research, development, and industrial applications. The first type is using carbon based electrodes and operating without faradaic processes in charging and discharging. For this type of supercapacitors, activated carbon has been the material of choice for nearly forty years since it was first developed for commercial applications in early 1980s [4,5]. These supercapacitors are based on the mechanism of electrochemical double-layer capacitance. They store the electric charges electrostatically by using reversible adsorption of ions of the electrolyte onto electrodes that are electrochemically stable and have high accessible surface area [6]. Very recently, carbon nanotubes, graphene, and their composites have also been investigated for improving the performance of such supercapacitors [7–11]. A

* Corresponding author.
** Corresponding author. National Institute for Materials Science, 1-2-1 Sengen, Tsukuba 305-0047, Japan
E-mail addresses: q-cheng@cq.jp.nec.com (Q. Cheng), tang.jie@nims.go.jp (J. Tang), shinya.norio@nims.go.jp (N. Shinya), lcqin@email.unc.edu (L.-C. Qin).

0378-7753/$ – see front matter © 2013 Elsevier B.V. All rights reserved.
http://dx.doi.org/10.1016/j.jpowsour.2013.04.105

record high energy density of 155 Wh kg^{-1} has recently been obtained by using graphene and single-walled carbon nanotube (CNT) composite electrodes in symmetric supercapacitors [7]. The second type of supercapacitors is oxidation–reduction based electrochemical capacitors where transition metal oxides, such as MnO_2 and RuO_2, are utilized for fast and reversible redox reactions to take place at the surface of active materials [12–19]. The metal oxide usually has a high specific capacitance but often suffers from poor power performance due to its relatively high electrical resistance. The third type of supercapacitors is based on conductive polymers such as polyaniline and polypyrrole [20–24]. The conductive polymers offer a high specific capacitance and low production cost, though the conductive polymer based supercapacitors usually have poor stability during cycling because of the destabilization of the polymeric backbone structure.

To compare the various carbon materials currently investigated for supercapacitor applications, Fig. 1 summarizes their pros and cons schematically. Among all carbon materials, activated carbon is the most popular electrode material for supercapacitors due to its large specific surface area and low production cost and it has been the material of choice for nearly four decades. However, in activated carbon there is usually a large fraction of carbon atoms that cannot be accessed by the electrolyte ions as illustrated in Fig. 1a. These carbon atoms are not utilized effectively in terms of activating their electrochemical functions. This is a major factor that limits the specific capacitance of activated carbon electrodes. Moreover, the low electrical conductivity of activated carbon is also limiting its applications in high power density supercapacitors and results in a low specific capacitance per area. Carbon nanotubes, especially single-walled carbon nanotubes (CNTs), on the other hand, have shown much improved electrical conductivity and large readily accessible surface area. However, CNTs are very likely to form bundles. As a result, only the outermost portion of a CNT bundle can function for ion absorption and the inner carbon atoms are all "wasted" electrochemically as illustrated in Fig. 1b and this is largely responsible for the lower specific capacitance of CNT-based supercapacitors. To overcome the shortcomings of activated carbon and carbon nanotubes as discussed above, graphene offers a most attractive alternative [25]. Graphene and chemically modified graphene sheets possess a high electrical conductivity, large specific surface area, and outstanding mechanical properties comparable with or even better than CNTs [26]. The specific surface area of a single graphene is 2630 $m^2\ g^{-1}$, which is much larger than that of activated carbon and carbon nanotubes that are usually used in the electrochemical double-layer capacitors [10,26–30]. However, graphene nano-sheets tend to form irreversible agglomerates or even re-stack to form graphite through van der Waals interactions during the process of drying. Moreover, the chemically reduced graphene usually has an electrical conductivity of about 100–200 S m^{-1}, which is two orders of magnitude lower than conductive CNTs (typically 10,000 S m^{-1}) [30], and cannot be made into electrodes without using binders. Fig. 1d shows schematically the cations and anions of ionic liquid 1-ethyl-3-methyl imidazoliumbis(trifluoromethanesulfone)imide (EMI-TFSI) used in this study. In this case, it would be difficult for the ions of size around 0.8 nm to gain access to the inner layers of graphene to form electrochemical double-layers if the graphene sheets are stacked together. Instead, the ions can only accumulate on the outmost layer of the graphene sheets and would then result in a lower specific capacitance [31], as illustrated in Fig. 1c.

We have recently proposed and developed graphene/CNT composite electrodes with a three-dimensional network structure that exhibited a record high energy density of 155 Wh kg^{-1} and maximum power density of 263 kW kg^{-1} when they were used in symmetric supercapacitors [7]. On the other hand, the specific capacitance as well as energy density will be further increased if we can decorate the graphene/CNT electrodes with active materials such as metal oxides or conductive polymers. The conductive polymer of polyaniline (PANI) has advantages in terms of low-cost, ease of synthesis, good stability in air, high conductivity, and high theoretical specific capacitance [32]. The PANI used in supercapacitors usually has excellent electrochemical properties with a specific capacitance of 233–1220 F g^{-1} [11,33–35]. As a result, PANI based supercapacitors could offer a high-performance and low-cost alternative for energy storage for applications such as electrical vehicles and high power tools [36].

Our strategy is shown schematically in Fig. 2. First, we use graphene and CNT suspensions (Fig. 2a) to prepare graphene/CNT composite by sonication and vacuum filtration. The graphene/CNT composite has high electric conductivity, chemical stability, and

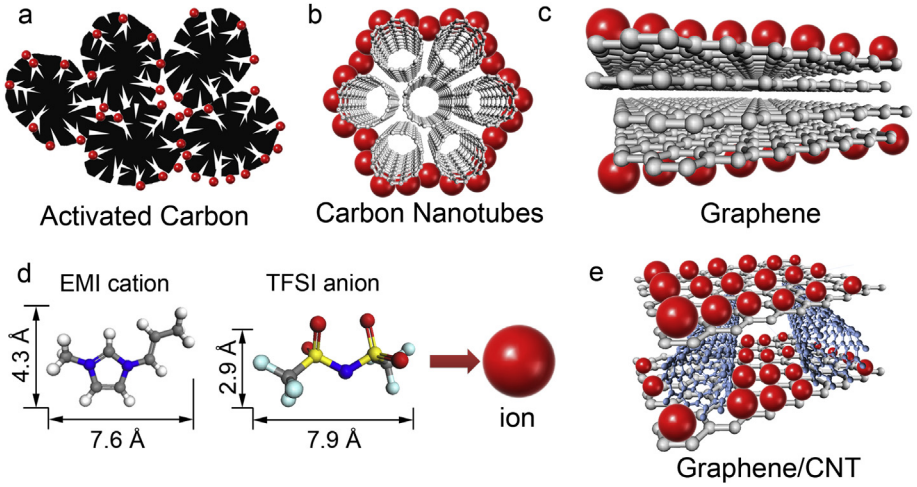

Fig. 1. Comparison of various carbon structures as electrode material for supercapacitors. a) Activated carbon. Activated carbon has high specific surface area, but the electrical conductivity is low. The micropores and interior atoms are usually inaccessible to organic or ionic liquid electrolyte ions. b) Single-walled carbon nanotubes (CNTs). CNTs are likely to attract each other through van der Waals interactions forming bundles. It is difficult for electrolyte ions to access the nanotubes beneath the surface ones. c) Graphene. Two-dimensional graphene nano-sheets can agglomerate easily during the drying process. The electrolyte ions could only absorb on the outermost surface of graphene nanoplatelets. d) Models of the structure of EMI and TFSI ions show a size correlation. e) Graphene/CNT composite. CNTs can serve as a spacer in between the graphene nano-sheets resulting rapid diffusion pathways for the electrolyte ions. Moreover, they can enhance electrical conduction for the electrons. CNTs can also serve as a binder to hold the graphene nano-sheets together while preventing disintegration of the graphene structure into the electrolyte.

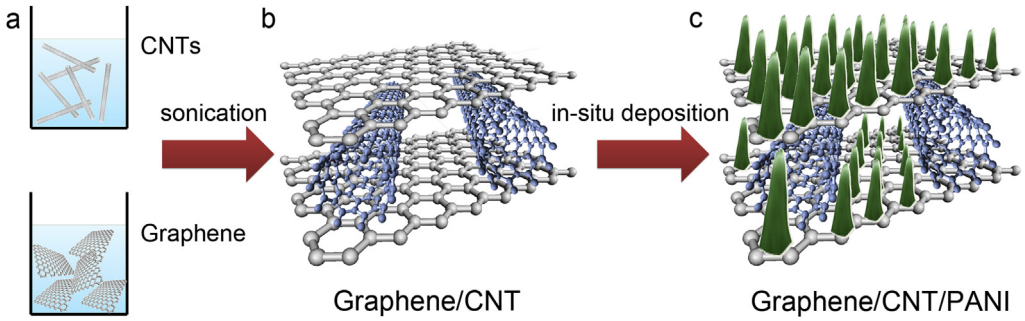

Fig. 2. Illustration of fabrication of graphene/CNT and graphene/CNT–PANI composites. a) Graphene and CNTs are first suspended in ethanol. b) Graphene and CNT suspensions are mixed together by sonication and then made into graphene/CNT composite by vacuum filtration. c) Graphene/CNT paper is coated with vertically aligned PANI nano-cones by anodic in-situ deposition to make graphene/CNT–PANI composite.

three-dimensional structure with high porosity as illustrated in Fig. 2b. The porous structure of graphene/CNT composite is therefore expected to facilitate the diffusion of electrolyte ions into the electrodes and to provide channels for rapid ions transport. Vertically aligned PANI nano-cones are then coated onto the graphene/CNT composite by electrodeposition as illustrated in Fig. 2c. The PANI coated graphene/CNT composite electrodes are utilized without any binder in order to reduce the interfacial resistance and to increase the electrochemical reaction rate. The vertically aligned PANI nano-cones can improve the electric conduction and shorten ion diffusion path. The nanostructured PANI can also increase the efficiency of usage of electrode material since only the part within a few nanometres from the surface of active material can take part in the redox reactions and contribute to the actual device capacitance.

2. Experimental

2.1. Graphene oxide

Graphene oxide was synthesized by using a modified Hummers–Offeman method from graphite in our experiment [22]. Graphite and $NaNO_3$ were first mixed together in a flask before H_2SO_4 (95%) was added to the flask. Potassium permanganate was then added to the suspension. The colour of the suspension would become bright brown after stirring. The mixture was finally washed by rinsing with 5% HCl and then demonized water. After centrifugation, filtration, and drying in vacuum, graphene oxide was obtained in the form of powders.

2.2. Reduction of graphene oxide

Graphene oxide was first dispersed in distilled water and sonicated. The suspension was then heated and hydrazine hydrate was added into the suspension. The reduced graphene was collected by filtration in the form of black powders. The obtained material was finally washed using distilled water again to remove the excessive hydrazine.

2.3. Preparation of graphene/CNT–PANI composite

To make the graphene/CNT–PANI composite, graphene and CNTs were first dispersed and mixed in ethanol with concentration of 0.08 mg ml^{-1} for graphene and 0.02 mg ml^{-1} for CNTs and followed by sonication of 30 min to obtain a uniform graphene/CNT composite film by vacuum filtration using a PTFE filter paper of 250 nm in porosity. Electrodeposition of PANI was conducted using a three-electrode system and a platinum sheet was used as the counter electrode. Anodic deposition was controlled by a potentiostat in HCl electrolyte containing aniline monomers [23]. The PANI nano-cones were synthesized in two steps: (i) nucleation of PANI, obtained at a constant potential, and (ii) growth of the PANI nano-cones obtained at a constant current.

2.4. Electrochemical and structure characterization

The electrochemical properties and capacitance of the supercapacitor electrodes, of gravimetric density of 0.4 mg cm^{-2} and assembled in coin cells (CR2032, Hohsen Corp.) in both symmetric and asymmetric configurations, were studied in a two-electrode setup by cyclic voltammetry (CV), galvanostatic charge and discharge, and electrochemical impedance spectroscopy (EIS). The CV response of the electrodes was measured at different scan rates varying from 10 to 100 mV s^{-1}. The voltammetric testing was carried out at potentials between 0 and 0.9 V in 1 M KCl aqueous electrolyte solution. The graphene/CNT and graphene/CNT–PANI composites were also studied in the ionic liquid of 1-ethyl-3-methylimidazoliumbis(trifluoromethanesulfone)imide (EMI-TFSI) with charging voltage of 4 V. EIS measurements were carried out without DC bias sinusoidal signal of 0.005 V over the frequency range from 100 kHz to 0.1 Hz. The morphologies and nanostructure of the materials were examined using both scanning electron microscopy (SEM, JSM-6500) and transmission electron microscopy (TEM, JEM-2100).

3. Results and discussion

Fig. 3 shows the morphologies and structure of graphene, graphene/CNT composite, and graphene/CNT with nano-PANI coating. Fig. 3a displays the morphology of the as-synthesized graphene, in which thin sheets of graphene are clearly resolved. A low magnification TEM image of graphene is shown in Fig. 3b. It can be seen that this few-layer graphene is thin and flat, which is essential for achieving a high value of specific surface area. A high-resolution TEM image of the few-layer graphene is given in Fig. 3c, in which we can see clearly that it is a triple-layer graphene. A more definitive identification of graphene was made by an analysis of the electron diffraction pattern shown in the inset of Fig. 3c. The spot pattern has the typical six-fold rotational symmetry expected for graphite and graphene. The {110}* reflections are more intensive than the {100}* reflections, indicating that it is a multilayer graphene [37]. Fig. 3d is a TEM image of the graphene/CNT composite. We can observe that the CNTs are very long and they are entangled to form a structure similar to a spider web. This kind of web-like structure should help hold together the graphene nano-sheets or other structures that are in contact with it. The CNTs used in this structure have higher electrical conductivity than the chemically

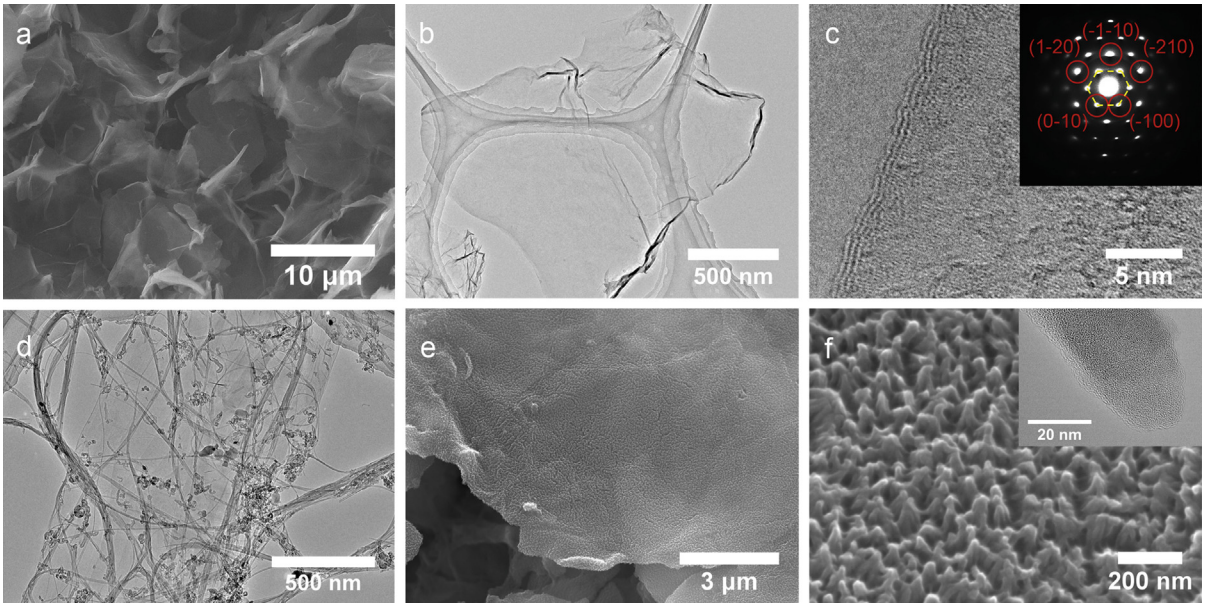

Fig. 3. Morphological and structural characterization of various carbon structures. a) SEM image of as-synthesized graphene. b) TEM image of graphene at low magnification. c) High-resolution TEM image of graphene. Inset is an electron diffraction pattern acquired from the graphene sheet. d) TEM image of graphene/CNT composite. e) SEM image of graphene/CNT composite with PANI coating at low magnification. f) SEM image of PANI coating at high magnification. Inset is a TEM image of a PANI nano-cone.

reduced graphene and in effect the electrical resistance of the electrode would be reduced, i.e., the CNTs act as the "pathways" for electrical conduction. In addition, the CNTs can also serve as a spacer in between the graphene nano-sheets to improve ion accessibility. Fig. 3e is an SEM image after PANI coating. The PANI nano-cones were grown on the graphene sheet quite uniformly. We controlled the thickness of PANI coating by adjusting the coating time. A high-resolution SEM image of the PANI nano-cones is given in Fig. 3f, showing the uniform coating of PANI. The diameter of the nano-cones is measured to be around 35 nm from the TEM images and a typical image is shown in the inset.

The capacitance of a supercapacitor is strongly dependent on the cell configuration set for the electrochemical measurement and it is always significantly higher when using a three-electrode system [21]. A two-electrode test cell was therefore used in this work because it can provide the most accurate measurement of the material performance for the supercapacitor [22]. In our experiment we assembled coin cells in both symmetric configuration (same material and format for both electrodes) and asymmetric configuration (graphene/CNT–PANI as cathode and graphene/CNT as anode). The supercapacitors were tested in two different electrolytes that are used routinely for supercapacitors. The aqueous electrolyte is 1 M KCl and the ionic liquid electrolyte is EMI-TFSI. For comparison Fig. 4a shows the charge and discharge curves of activated carbon, CNTs, graphene, and graphene/CNT composite electrode in symmetric configuration in 1 M KCl electrolyte. These carbon materials store the energy based on the electric double-layer capacitance, which mainly depends on the effective surface area. We can learn from Fig. 4a that the graphene/CNT composite electrode exhibited the highest capacitance. Fig. 4b shows the CV curves of graphene/CNT composite in EMI-TFSI at different scan rates ranging from 10 to 200 mV s^{-1}. The symmetric and nearly rectangular shape of the CV curves indicates excellent charge propagation in the electrodes. As we know, the shape of the CV loop of an ideal capacitor should be rectangular if the contact resistance is small. Larger resistance distorts the loop and results in a narrower loop with an oblique angle. Fig. 4c shows the specific capacitance of graphene/CNT composite electrode at different charging current densities from 0.3 to 6.3 A g^{-1}. The average specific capacitance reached 271.0 F g^{-1} at the charging current density of 0.3 A g^{-1}. The specific capacitance reached 134.5 F g^{-1} even at a very large current density of 3.1 A g^{-1}. The graphene/CNT composite preserved 60% of its specific capacitance in EMI-TFSI ionic liquid electrolyte when the current density increased from 0.3 to 2.0 A g^{-1}. To study the effects of PANI coating on the capacitance of the electrode, PANI nano-cones were coated onto the graphene/CNT composite described above at three coating densities of 0.4, 0.6, and 0.8 mg cm^{-2}, among which the highest specific capacitance was achieved at coating density of 0.6 mg cm^{-2}. To evaluate the device performance, a single graphene/CNT–PANI electrode (weight 3.5 mg and diameter 1.0 mm) was assembled with a graphene/CNT electrode (weight 5.0 mg and diameter 1.2 mm) with a capacitance ratio of 1:1.2 as adapted in battery testing to construct an asymmetric supercapacitor. All tests were performed at a stable room temperature of about 25 °C. The improvement of electrode performance with PANI coating is demonstrated in Fig. 4d, where the CV curves of graphene/CNT composite are shown before and after the PANI coating with coating density of 0.6 mg cm^{-2}. The CV current increased significantly after the PANI coating, indicating an increase in the capacitance attributed to the PANI coating and redox reactions due to PANI. Fig. 4e is the Nyquist plot of impedance collected in the frequency range between 100 kHz and 0.1 Hz for the graphene/CNT composite before and after PANI coating. As expected from a supercapacitor, at low frequency, the imaginary part increased sharply and a nearly vertical line is observed, indicating a pure capacitive behaviour. As the frequency increased, the influence of the electrode porosities was observed as indicated by a constant phase element typified by the Warburg curve [38]. Both EIS curves shown in Fig. 4e are nearly linear in the low frequency region and have a semi-circle in the high frequency region, from which the faradaic leakage resistance, R_F, due to overcharge or faradaic redox reactions caused by impurities or functional groups, can be inferred to. A smaller R_F corresponds to greater kinetic reversibility of the faradaic reactions. In a practical supercapacitor, to a good approximation, it can be regarded as composed of a non-faradaic current for electrochemical double-layer charging in

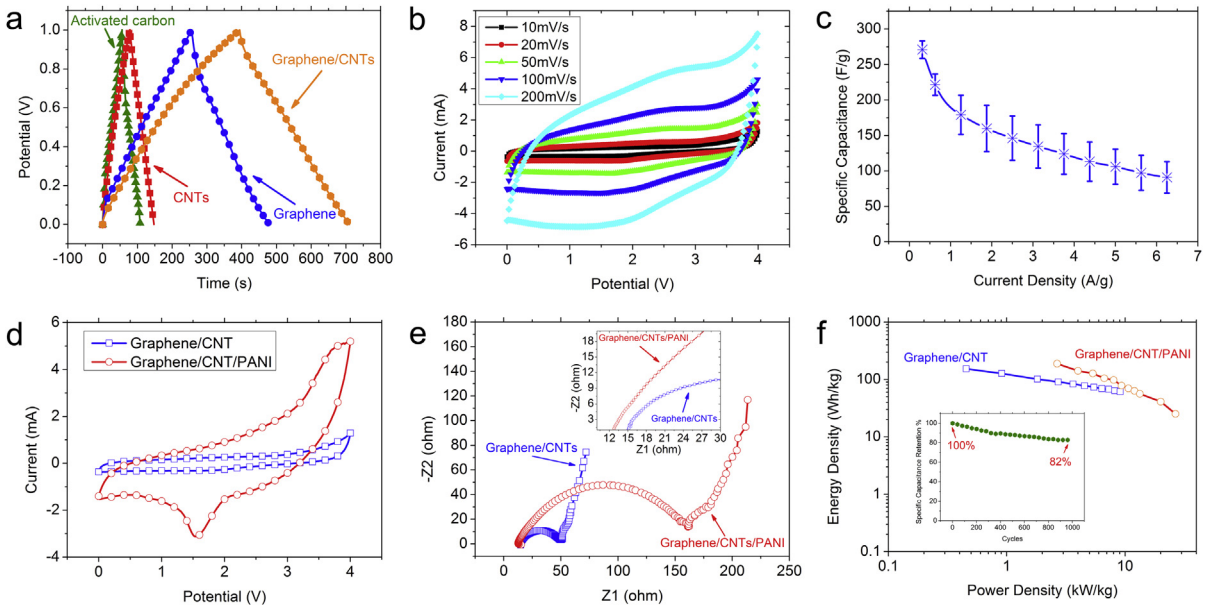

Fig. 4. Electrochemical properties of graphene/CNT based electrodes. a) Galvanostatic charge/discharge curves in 1 M KCl electrolyte of activated carbon, single-wall carbon nanotubes, graphene, and graphene/CNT composite at charging density of 1 A g^{-1}. b) CV curves of graphene/CNT composite at different scan rates from 10 to 200 mV s^{-1} in EMI-TFSI electrolyte. c) Specific capacitance of graphene/CNT composite electrode at different charging current densities. d) CV curves of the graphene/CNT composite electrode before and after PANI coating. e) Nyquist plot of the EIS data of graphene/CNT and graphene/CNT–PANI composite electrodes. Inset is an enlarged portion at highest frequency. f) Ragone plot of graphene/CNT and graphene/CNT–PANI composite electrodes. Inset is the cycling performance of graphene/CNT–PANI at charging density of 2 A g^{-1}.

parallel with some faradaic current component through R_F. By comparing the diameter of the semi-circles shown in Fig. 4e, we can learn that the graphene/CNT composite has a smaller charge transfer resistance than the graphene/CNT–PANI composite. The equivalent series resistance (ESR) of the graphene/CNT electrode and the graphene/CNT–PANI electrode was also obtained from the Z1-intercept as shown in the inset of Fig. 4e, and they are 14.8 and 13.3 Ω, respectively. We noticed that the ESR decreased after we made PANI coating on the graphene/CNT electrode. This is because the graphene and CNTs are stacked together and the points of contact of the two components may increase the electric resistance, while the PANI coating would enlarge the contact area and therefore would in turn reduce the electric resistance. The maximum power density p_{max} can be calculated $p_{max} = V_{max}^2/(4mR_{ESR})$, where R_{ESR} is the equivalent series resistance, m is the total weight of the two electrodes, and V_{max} is the maximum charging voltage. Using V_{max} = 4 V for the EMI-TFSI electrolyte, the obtained maximum power densities for the graphene/CNT and graphene/CNT–PANI electrodes are 270.3 and 200.5 kW kg^{-1}, respectively.

The Ragone plot which maps the energy density and power density is shown in Fig. 4f. The average energy density and power density were calculated according to equations (1) and (2) given below:

$$E_{density} = \frac{1}{2} C_{sp} V_{max}^2 \quad (1)$$

and

$$P = \frac{E_{density}}{\Delta t} \quad (2)$$

where $E_{density}$ is energy density of the supercapacitor, C_{sp} is the total specific capacitance, V_{max} is the maximum charging voltage, and Δt is the discharge time [31,39]. In the present study, the highest energy density for the graphene/CNT is 150.6 Wh kg^{-1} with a power density of 0.5 kW kg^{-1} and the highest power density for graphene/CNT is 9.1 kW kg^{-1} with an energy density of 61.1 Wh kg^{-1}. For the asymmetric supercapacitor with one graphene/CNT–PANI electrode, we obtained the highest energy density of 188.4 Wh kg^{-1} with a power density of 2.7 kW kg^{-1} and the highest power density of 26.7 kW kg^{-1} with an energy density of 25.1 Wh kg^{-1}. The inset of Fig. 4f shows the cycling performance of the asymmetric supercapacitor with PANI coating of 0.6 mg cm^{-2} at charging current density of 2 A g^{-1} and charging voltage up to 4 V. The capacitance dropped 18% after 1000 cycles, indicating good cyclability of the electrodes.

The outstanding performance of the supercapacitor electrodes studied in this work is attributed to a synergetic combination of properties of graphene and CNTs. Graphene has the largest theoretical electrochemical double layer capacitance of about 526 F g^{-1}. However, even the highest reported experimental measurement could only attain 25%–40% at best of this theoretical value. A major problem is the re-stacking of graphene sheets. Ions, especially larger organic ions, may have difficulty in accessing the electrode. On the other hand, CNTs have a very high electrical conductivity of 10,000 S m^{-1} which is two orders of magnitude larger than chemically reduced graphene nano-sheets. Therefore the use of CNTs can reduce the internal electrical resistance of the electrode to improve the power performance. The CNTs should also have functioned as spacers to prevent graphene nano-sheets from re-stacking or agglomeration and therefore to improve the accessibility for electrolyte ions. The electrodes would be accessed more effectively by the electrolyte ions with the assistance of CNT spacers to allow more active material to be utilized electrochemically as illustrated in Fig. 1e. In addition, the CNTs have excellent binding properties to serve also as binder to hold together the graphene nano-sheets.

4. Conclusions

We have fabricated and studied graphene/CNT and graphene/CNT–PANI electrodes for asymmetric supercapacitors. The single-walled carbon nanotubes (CNTs) act as a conductive spacer as

well as conductive binder in this composite structure. A highest energy density of 188.4 Wh kg^{-1} and maximum power density of 200.5 kW kg^{-1} have been obtained. The vertically aligned PANI nano-cones are suggested to increase the electric conduction and utilization of active material which lead to significant increase of the specific capacitance that is highly desirable for applications in hybrid or pure electric vehicles. Furthermore, the results are also potentially useful for preparation of other graphene-based composites to meet diverse application requirements imposed on supercapacitors.

Acknowledgement

This work was supported by JSPS Grants-in-Aid for Scientific Research No. 19310081 and 22310074, JST ALCA Program, and the Nanotechnology Network Project of the Ministry of Education, Culture, Sports, Science and Technology (MEXT), Japan.

References

[1] P. Simon, Y. Gogotsi, Nat. Mater. 7 (2008) 845–854.
[2] J.R. Miller, P. Simon, Science 321 (2008) 651–652.
[3] L.L. Zhang, X.S. Zhao, Chem. Soc. Rev. 38 (2009) 2520–2531.
[4] E. Frackowiak, F. Beguin, Carbon 39 (2001) 937–950.
[5] E. Frackowiak, F. Beguin, Carbon 40 (2002) 1775–1787.
[6] A.G. Pandolfo, A.F. Hollenkamp, J. Power Sources 157 (2006) 11–27.
[7] Q. Cheng, J. Tang, J. Ma, H. Zhang, N. Shinya, L.-C. Qin, Phys. Chem. Chem. Phys. 13 (2011) 17615–17624.
[8] D.N. Futaba, K. Hata, T. Yamada, T. Hiraoka, Y. Hayamizu, Y. Kakudate, O. Tanaike, H. Hatori, M. Yumura, S. Iijima, Nat. Mater. 5 (2006) 987–994.
[9] Y. Wang, Z.Q. Shi, Y. Huang, Y.F. Ma, C.Y. Wang, M.M. Chen, Y.S. Chen, J. Phys. Chem. C 113 (2009) 13103–13107.
[10] M.D. Stoller, S.J. Park, Y.W. Zhu, J.H. An, R.S. Ruoff, Nano Lett. 8 (2008) 3498–3502.
[11] D.W. Wang, F. Li, J.P. Zhao, W.C. Ren, Z.G. Chen, J. Tan, Z.S. Wu, I. Gentle, G.Q. Lu, H.M. Cheng, ACS Nano 3 (2009) 1745–1752.
[12] A.E. Fischer, K.A. Pettigrew, D.R. Rolison, R.M. Stroud, J.W. Long, Nano Lett. 7 (2007) 281–286.
[13] J.K. Chang, M.T. Lee, W.T. Tsai, M.J. Deng, H.F. Cheng, I.W. Sun, Langmuir 25 (2009) 11955–11960.
[14] B. Babakhani, D.G. Ivey, J. Power Sources 195 (2010) 2110–2117.
[15] Q. Cheng, J. Tang, J. Ma, H. Zhang, N. Shinya, L.-C. Qin, Carbon 49 (2011) 2917–2925.
[16] B.E. Conway, J. Electrochem. Soc. 138 (1991) 1539–1548.
[17] J.W. Long, K.E. Swider, C.I. Merzbacher, D.R. Rolison, Langmuir 15 (1999) 780–785.
[18] J. Yan, Z.J. Fan, T. Wei, W.Z. Qian, M.L. Zhang, F. Wei, Carbon 48 (2010) 3825–3833.
[19] G.R. Li, Z.P. Feng, Y.N. Ou, D.C. Wu, R.W. Fu, Y.X. Tong, Langmuir 26 (2010) 2209–2213.
[20] K.S. Ryu, K.M. Kim, N.G. Park, Y.J. Park, S.H. Chang, J. Power Sources 103 (2002) 305–309.
[21] E. Frackowiak, V. Khomenko, K. Jurewicz, K. Lota, F. Beguin, J. Power Sources 153 (2006) 413–418.
[22] V. Khomenko, E. Frackowiak, F. Beguin, Electrochim. Acta 50 (2005) 2499–2506.
[23] J.H. Park, J.M. Ko, O.O. Park, D.W. Kim, J. Power Sources 105 (2002) 20–25.
[24] J. Li, L. Cui, X.G. Zhang, Appl. Surf. Sci. 256 (2010) 4339–4343.
[25] J.C. Meyer, A.K. Geim, M.I. Katsnelson, K.S. Novoselov, T.J. Booth, S. Roth, Nature 446 (2007) 60–63.
[26] H.A. Becerril, J. Mao, Z. Liu, R.M. Stoltenberg, Z. Bao, Y. Chen, ACS Nano 2 (2008) 463–470.
[27] V.C. Tung, M.J. Allen, Y. Yang, R.B. Kaner, Nat. Nanotechnol. 4 (2009) 25–29.
[28] S. Stankovich, D.A. Dikin, G.H.B. Dommett, K.M. Kohlhaas, E.J. Zimney, E.A. Stach, et al., Nature 442 (2006) 282–286.
[29] A.K. Geim, P. Kim, Sci. Am. 298 (2008) 90–97.
[30] S. Park, R.S. Ruoff, Nat. Nanotechnol. 4 (2009) 217–224.
[31] J. Yan, T. Wei, B. Shao, Z.J. Fan, W.Z. Qian, M.L. Zhang, F. Wei, Carbon 48 (2010) 487–493.
[32] J.C. Lacroix, A.F. Diaz, J. Electrochem. Soc. 135 (1988) 1457–1463.
[33] H. Zhang, G.P. Cao, Z.Y. Wang, Y.S. Yang, Z.J. Shi, Z.N. Gu, Electrochem. Commun. 10 (2008) 1056–1059.
[34] S.R. Sivakkumar, W.J. Kim, J.A. Choi, D.R. MacFarlane, M. Forsyth, D.W. Kim, J. Power Sources 171 (2007) 1062–1068.
[35] V. Gupta, N. Miura, J. Power Sources 157 (2006) 616–620.
[36] J.M. Tarascon, M. Armand, Nature 414 (2001) 359–367.
[37] Y.V. Hernandez Nicolosi, M. Lotya, F.M. Blighe, Z.Y. Sun, Y. De, et al., Nat. Nanotechnol. 3 (2008) 563–568.
[38] C. Portet, P.L. Taberna, P. Simon, C. Laberty-Robert, Electrochim. Acta 49 (2004) 905–912.
[39] J. Yan, T. Wei, B. Shao, F.Q. Ma, Z.J. Fan, M.L. Zhang, C. Zheng, Y.C. Shang, W.Z. Qian, F. Wei, Carbon 48 (2010) 1731–1737.